



Microfluidic platform for encapsulation of plant extract in chitosan microcarriers embedding silver nanoparticles for breast cancer cells

Ayesha Aftab¹ · Shazia Bashir² · Saima Rafique³ · Tayyaba Ghani⁴ · Ranjha Khan⁵ · Muhammad Bashir² · Aiman Ehsan¹ · Malik Ihsanullah Khan⁶ · Atta Ullah Shah⁷ · Arshad Mahmood⁷

Received: 2 March 2020 / Accepted: 24 April 2020 / Published online: 6 May 2020
© King Abdulaziz City for Science and Technology 2020

Abstract

In this study, the controlled synthesis of microcarriers and CpE loading were aimed to achieve by microfluidic system. The effect of temperature on chitosan in the stabilization of silver nanoparticles, microcarrier size and the encapsulation efficiency was measured. Encapsulation was achieved by the controlled rapid mixing in polymethyl-methacrylate (PMMA) microfluidic chip. The CpE was found to contain primary and secondary phenols in the phytochemical screening. The capping property of chitosan was achieved by heating reaction mixture in polytetrafluoroethylene (PTFE) tube to get the stabilized silver nanoparticles which were found to be embedded in chitosan microspheres of size 23.7 μm on average. Fourier-transform infrared (FTIR) and ultraviolet–visible (UV–Vis) spectroscopy results indicated the successful encapsulation of CpE in microcarriers. The average percentage encapsulation efficiency (% EE) of CsAg was found to be $77.125 \pm 6.9\%$. The CpE-loaded microcarriers had shown significant anti-oxidant activity ($p < 0.01$). CpE-loaded microcarriers were evaluated to have robust cytotoxicity against 4T1 breast cancer cells at very low dose ($\text{IC}_{50} = 42.53 \mu\text{g/mL}$), which inhibited 95% of cancer cells viability. These results confer that microfluidic system plays an important role in the formation of CpE-loaded CsAg microcarriers that could effectively ($p < 0.0001$) kill the breast cancer cells.

Keywords Chitosan silver microcarriers · Plant extract · Microfluidic system

Electronic supplementary material The online version of this article (<https://doi.org/10.1007/s13204-020-01433-8>) contains supplementary material, which is available to authorized users.

✉ Shazia Bashir
shazia@pieas.edu.pk

- ¹ Department of Biological Sciences, International Islamic University, Islamabad 44000, Pakistan
- ² Microsystems Laboratory, Department of Physics and Applied Mathematics, Pakistan Institute of Engineering and Applied Sciences (PIEAS), Islamabad, Pakistan
- ³ Department of Physics, Air University, Islamabad, Pakistan
- ⁴ Department of Metallurgy and Material Engineering, PIEAS, Islamabad 45650, Pakistan
- ⁵ Department of Biotechnology and Bioinformatics, Quaid-I-Azam University, Islamabad, Pakistan
- ⁶ Division of Molecular Medicine, Hefei National Laboratory for Physical Sciences At Microscale, School of Life Sciences, University of Science and Technology of China, Hefei 230026, China
- ⁷ National Institute of Laser and Optronics (NILOP), Islamabad 44000, Pakistan

Introduction

Extensive research has been conducted to prepare different types of nanoparticles, such as metallic, polymeric and ceramic nanoparticles. Owing to unique physical and chemical properties, they are playing a vital role in the materials technology, such as manufacturing of nanodevices (Hoseinzadeh et al. 2017a; Najafi-Ashtiani et al. 2018; Hoseinzadeh and Ramezani 2019), nanofluids (Sarafraz et al. 2014; Salari et al. 2016, 2017; Yousefzadeh et al. 2019; Ellahi et al. 2020), thin films (Hoseinzadeh et al. 2017b, 2018) and in biomedical applications particularly drug delivery (Jacob et al. 2020). The uniform dispersion of nanoparticles in different solvents form nanosuspension, which has diverse applications (Sarafraz and Arjomandi 2018a, b). It has been well established that the pharmaceutical nanosuspensions consist of uniformly distributed nanoparticles which act as nano-carriers to encapsulate the drug in order to provide a long shelf life and a safe targeted delivery of the drug in human body for cancer therapy (Jacob et al. 2020).

The recent research not only focuses on nano-scale carriers for the encapsulation of natural drugs but also demonstrates a wide range of applications for microcarriers or microspheres as drug carriers (Medina-Sánchez et al. 2018; Zugic et al. 2020). These microscale carriers have also been studied to give robust anti-cancer properties by showing the enhanced cell penetration and cellular uptake through endocytosis at the targeted cell site just like nano-carriers (Huang et al. 2010; Munin and Edwards-Lévy 2011; Adhikari and Yadav 2018). Among these microcarriers, polymeric particles are the best studied carriers of drug due to their biocompatible properties and controllable drug delivery system (Kong et al. 2013). The biodegradable polymeric microspheres prepared by poly DL-lactide-co-glycolide (PLGA) and poly vinyl alcohol (PVA) have been reported for a localized delivery for breast cancer therapy (Obayemi et al. 2014). The chitosan, for example, has been working efficiently as nano and microcarrier of hydrophilic drug from ages (Nair et al. 2009; Li et al. 2018).

Chitosan, a naturally occurring polysaccharide has gained keen interest in medicine because of its desirable features including biodegradability, biocompatibility and non-toxicity (Stoica et al. 2013; Kummari et al. 2015; Hussein-Al-Ali et al. 2018). In biomedical fields, it has been used for wound healing, tissue engineering and drug delivery (Hussein-Al-Ali et al. 2018). In combination with silver nanoparticles is emerging as an efficient composite for diverse medical applications (Yang et al. 2016; Palem et al. 2018; Nate et al. 2018). The chitosan and its derivatives have shown excellent anti-tumour effects due to their anti-oxidative properties and scavenging of cancer causing free radicals (Adhikari and Yadav 2018).

The uncontrolled division of abnormal cells in breast tissues is called the breast cancer which is spreading in women worldwide (American Cancer Society 2019). Surgery, chemotherapy, targeted therapy and hormone therapy are the unaffordable treatment options for breast cancer with the survival rate of just up to 5 years (American Cancer Society 2019). This leads the world of pharmacopoeia to develop the affordable, efficient and precise medicinal plants to fight against the complex disease, such as cancer. One remedy lies in *Calotropis procera* which is a xerophytic, evergreen, erect, perennial shrub and a flowering plant. It grows widely in the tropical and sub-tropical areas of Africa and Asia including different areas of Pakistan like Balochistan, Sindh and Northern areas (Khanzada et al. 2008). *Calotropis procera* extract (CpE) produces many bioactive constituents such as phenolic acids, flavonoids, alkaloids, calotropin, uskerin and calotaxein. These plant extracted constituents have been reported to possess biological properties like anti-cancer, anti-oxidant, anti-apoptotic and anti-microbial activities (Farouk et al. 2016; Alzahrani et al. 2019). Novel *Calotropis procera* protein has been reported to suppress the tumour

growth in the breast cancer through the downregulation of NF- κ B pathway (Samy et al. 2012a). However, the bioavailability of pharmacologic phytochemicals present in the plant extract (including CpE) is very important for its efficacy. The availability of phytochemicals can be addressed to meet the clinical importance by developing a carrier system with the best bioefficacy, pharmacokinetics and bioavailability (Munin and Edwards-Lévy 2011). An efficient carrier system could be a nano or micro-sized biomaterial which will contribute towards the stability and controlled release of bioactive nutrients and non-nutrients in the diverse biological environment. Therefore, the chitosan microcarriers can be used as CpE-loading material. This edible microcarriers system not only provides a safe delivery of drug, but also constitute a targeted delivery in the complex human body (Kesente et al. 2017; Chandirika et al. 2018).

Numerous research studies have proposed different techniques for synthesis of chitosan–silver (CsAg) particles, such as the sol–gel reaction method, gamma irradiation synthesis and chemical or green synthesis. However, the fabrication of uniform particles in nano or microsize remains a challenge. Microfluidic system is an emerging technology for precise controlling and manipulating fluids to generate the monodispersed and size-controlled droplets (Yang et al. 2016; Amoyav and Benny 2018; Wang et al. 2018; Maslanka Figueroa et al. 2020). This system provides a microemulsion reactor which can be used to achieve the monodispersity of CsAg particles by the application of high-speed mixing (Amoyav and Benny 2018). The CsAg nanoparticles have been widely used for anti-tumour and anti-microbial effects. These nanocomposite films, modified with PVA, have been previously used for the encapsulation of curcumin for improved anti-bacterial activity (Vimala et al. 2011). To the best of our knowledge, no research has been performed on encapsulation of the *Calotropis procera* extract (CpE) in CsAg microcarriers using microfluidic system. The current study focuses on the one-step encapsulation of CpE in monodispersed CsAg particles and achievement of robust cytotoxicity against breast cancer cells.

Methodology

This study consists of preparation of plant extract, its analysis and designing a microfluidic setup for the encapsulation of plant extract in CsAg microcarriers. Furthermore, the anti-oxidant and anti-breast cancer activities of CpE-loaded CsAg microcarriers were carried out. The flowchart of the synthesis route is illustrated in Fig. 1.

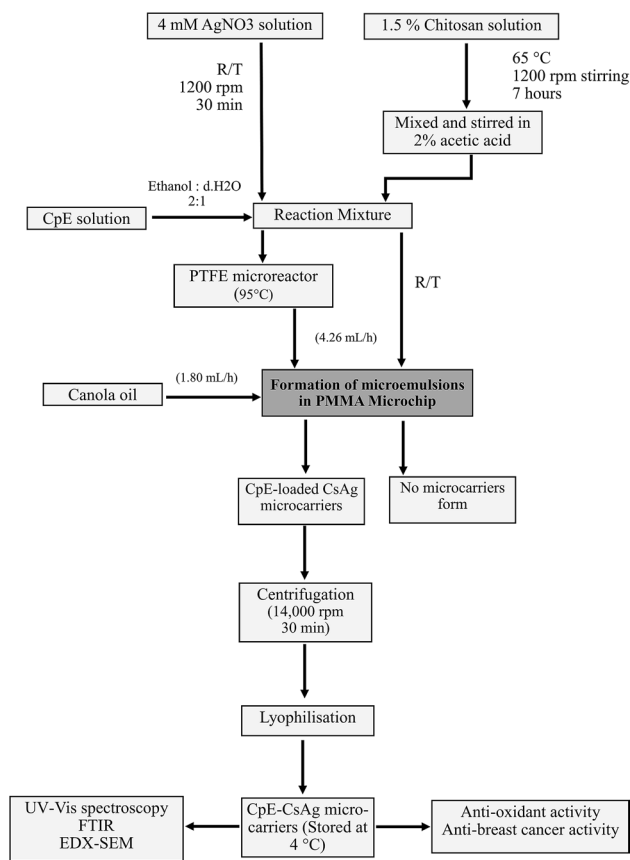


Fig. 1 Flow chart representing the steps taken for encapsulation of CpE in CsAg microcarriers and their biological analysis

Chemicals

Chitosan (low molecular weight, Sigma), silver nitrate (AgNO₃, Duksan), acetic acid, ethanol, de-ionized water (d.H₂O), canola oil (Sigma), hydrogen peroxide (H₂O₂), ascorbic acid, phosphate buffer (pH = 7.4), 3-(4,5-dimethylthiazol-2-yl)-2,5-diphenyltetrazolium bromide (MTT), dimethyl sulpho oxide (DMSO) and sodium hydroxide (NaOH). All these chemicals were of analytical grade.

Plant extract preparation and analysis

Medicinal plant collection

The *Calotropis procera* (NCBI: txid141467), was collected from Nilore, Islamabad, Pakistan owing to its importance as ethno botanical medicinal plant. The verification of the plant sample was definite by the Taxonomist and Herbarium of National Agriculture Research Council (NARC), Islamabad, Pakistan.

Preparation of extract

CpE was prepared using a combination of maceration and percolation extraction methods described before (Kaur 2018) with little modifications. The plant was washed with distilled water and dried under shade. The leaves of plant were separated and frozen overnight at $-20\text{ }^{\circ}\text{C}$. The leaves were immediately lyophilized and grinded afterwards to form a powder. The active components present in leaves were extracted with hydro-alcoholic solvent (menstruum), i.e. mixture of ethanol and d.H₂O (3:1). 50 g of plant powder was mixed in 100 mL of menstruum in an airtight container for 12 h using the shaker (Gallenkamp Model BKS-350) at 120 rpm and room temperature. Afterwards, the mixture was packed in percolator (having the opening at both ends) and menstruum was added to be passed through the plant material at a very low speed. Now this menstruum containing dissolved phytochemicals was collected from the outlet of percolator and more menstruum was poured from top until the collected sample was clear in colour. The mixture was subjected for filtration using Whatman filter paper (Grade 1 qualitative, 125 mm \varnothing) and filtrate was dried using the rotary evaporator (SENCO) at 30 °C. This dried ethanolic CpE was stored at 4 °C for further experimentations.

Preliminary qualitative phytochemical analysis

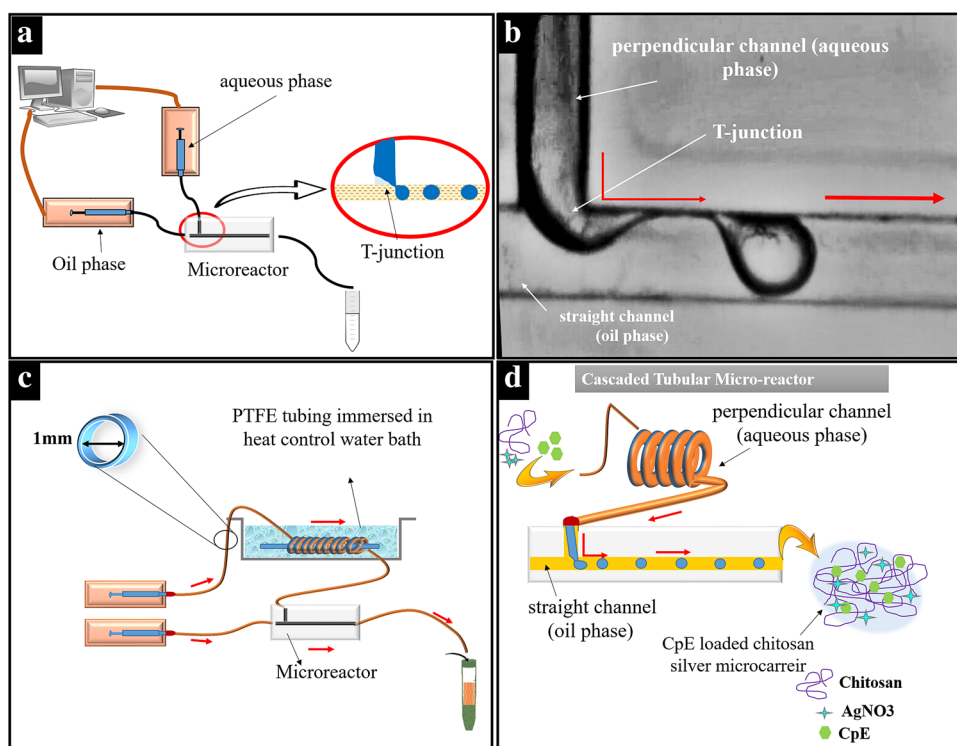
The phytochemical screening was executed to determine the active components extracted in ethanolic CpE. The qualitative biochemical tests were performed for analysis of terpenoids, alkaloids, flavonoids, tannins and phenols following the previous methodology (Gul et al. 2017). After confirmation of presence of essential phytochemicals, the extract was further processed for encapsulation and anti-cancer activity.

Microfluidic reactor for microcarriers synthesis and encapsulation

The experimental set-up for microfluidic synthesis is illustrated in Fig. 2. The T-shaped microfluidic reactor was fabricated on polymethyl-methacrylate (PMMA) using CNC machine (Shahzadi et al. 2018). The continuous oil phase (canola oil) was fed through the straight channel and the dispersed phase, consisting a mixture of silver nitrate solution, chitosan solution and CpE, was fed through the perpendicular channel.

The effective capping efficiency of chitosan for stabilization of metallic nanoparticles is achieved when chitosan is heated up to 95 °C as stated in previous reports (Akmaz et al. 2013; Nate et al. 2018; Mohan et al. 2019). However, PMMA chip cannot resist the higher temperature ($>90\text{ }^{\circ}\text{C}$) due to the depolymerization of PMMA that causes the channel blockage (Tsao and DeVoe 2009). Therefore, in the

Fig. 2 Experimental setup for synthesis of microcarriers and encapsulation of CpE. **a** The microfluidic system without heating. **b** T-junction image capture by camera-aided optical microscope during the formation of microemulsions. **c** PTFE tubular microfluidic reactor for heating the reaction mixture. **d** Cascaded tubular microreactor and the formation of CpE-loaded microcarriers. Red arrows showing the direction of flow of fluids, i.e. canola oil and reaction mixture consisted of AgNO_3 , CpE and chitosan. AgNO_3 silver nitrate, CpE *calotropis procera* extract, PTFE polytetrafluoroethylene



current study, the dispersed phase was heated up in helically coiled polytetrafluoroethylene (PTFE) tubing, which has high heat resistance (up to 260 °C (Hintzer et al. 2016)). This tubular reactor was immersed in temperature-controlled water bath to heat the reaction mixture up to 95 °C and it was cascaded with perpendicular channel of microchip in order to feed the heated mixture of the dispersed phase into the microchip. This study focused to synthesize the chitosan-stabilized silver nanoparticles and encapsulation of CpE using the microfluidic system.

Synthesis of CsAg microcarriers

The reaction mixture for CsAg microcarriers was prepared by mixing 1.5% of chitosan solution and 4 mM of AgNO_3 solution in volumetric ratio of 4:1, respectively. The CsAg microcarriers were prepared both at room temperature directly in microfluidic chip and also at 95 °C via a tubular reactor cascaded with microfluidic chip. The CsAg reaction mixture at room temperature as well as at elevated temperature (95 °C) was fed through a perpendicular channel and the continuous phase was fed through the straight channel of the microchip to form microemulsions as illustrated in Fig. 2. The flow rates of both dispersed and continuous phases were adjusted to form stable monodispersed microemulsions. The synthesized CsAg microcarriers were collected at the outlet of microfluidic chip in both cases and 10% of NaOH was added into the samples for further reduction. The samples were centrifuged at 10,000 rpm for 30 min to separate the

microcarriers from their colloidal solution. The resulting microcarriers were lyophilized and stored at room temperature for further analysis.

Synthesis of CpE-loaded-CsAg (CpE–CsAg) microcarriers

The CpE solution was prepared by dissolving 40 mg of CpE in 20 mL of solvent (2:3, ethanol: d.H₂O). The CpE was added into the reaction mixture of chitosan and AgNO_3 in volumetric ratios of 1, 2, 4 and 6 respectively. The CpE was loaded into the mixture of CsAg in both aforementioned cases prior to the emulsion formation in order to encapsulate the CpE in CsAg microcarriers. The collected samples were split into two equal parts. 10% NaOH was added in one of the samples as a reducing agent. However, the other sample was left without NaOH in order to analyze the reducing property of CpE.

Encapsulation efficiency percentage (%EE)

The encapsulation efficiency of CsAg microcarriers was calculated by indirect method, i.e. by measuring the concentration of free CpE in samples. The samples were centrifuged at 10,000 rpm for 30 min and supernatant was subjected to ultraviolet–visible (UV–Vis) spectrophotometer (Shimadzu UV-1201) analysis. The absorption was measured at 340 nm for calculating the concentration of free CpE in supernatant. The %EE was then calculated using the Eq. 1:

$$\%EE = \frac{Con_i - Con_f}{Con_i} \times 100 \quad (1)$$

where Con_i is the concentration of total CpE added initially and Con_f is the concentration of free/unloaded CpE in supernatant.

Characterization

The physical characteristics analysis of microcarriers was performed by UV–Vis spectrophotometer. The morphology analysis of microcarriers was performed by field-emission scanning electron microscope (FESEM) equipped with energy-dispersive X-ray (EDX) spectrometer (TESCAN MAIA3) having 5 kV accelerating voltage. Whereas, Fourier-transform infrared (FTIR) spectroscopy (Nicolet 6700, USA) was performed for functional group analysis.

Anti-oxidant activities

Anti-oxidant activity was measured to identify and compare the ability of CpE and CpE–CsAg microcarriers to scavenge H_2O_2 . The assay was carried out by following the Ruch et al. (1989) method (Ruch et al. 1989) with little modifications. 4 mM of H_2O_2 solution was prepared in 50 mM of phosphate buffer (pH 7.4). CpE and CpE–CsAg microcarriers (10 mg/mL) were suspended again and diluted to the concentration of 60 $\mu\text{g/mL}$, 80 $\mu\text{g/mL}$, 100 $\mu\text{g/mL}$, 120 $\mu\text{g/mL}$, 140 $\mu\text{g/mL}$ and 160 $\mu\text{g/mL}$. Ascorbic acid (10 mg/mL) was used as standard. A 20 mL of H_2O_2 was added in each dilution of test sample. Absorbance was measured at 230 nm using UV–Vis spectrophotometer after 10 min, against a blank. The percentage of radical scavenging capacity (%RSC) of test samples was calculated using Eq. 2:

$$(\%)RSC = 1 - \frac{Abs_{\text{sample}}}{Abs_{\text{Control}}} \times 100 \quad (2)$$

where Abs_{Control} is absorbance of blank and Abs_{sample} is absorbance of test samples.

Cytotoxicity

The cytotoxic effect of CpE and CpE–CsAg microcarriers was evaluated. The 4T1 cells (5×10^3 per well) were seeded in 96 well plate and cultured for 24 h at 37 °C. Different formulations of microcarriers with increased concentration were added into the cells and incubated for next 24 h. Then, the medium was replaced with fresh medium and the cells were incubated for further 24 h. Afterwards, medium was removed, MTT (1 mg/mL) was added for 4 h and then DMSO (100 μL) was added to dissolve the formazan. Relative cell viabilities were measured by microplate reader

(Model 680, Bio-Rad) to determine the absorbance of each well at 570 nm.

Statistical analysis

The results were stated as mean, standard deviation (SD), 95% confidence interval (CI) and inhibition coefficient (IC_{50}). ANOVA test was also accessed. All the statistical analyses were performed using the GraphPad Prism V.6.01. Statistical significance was established when $*p < 0.05$, $**p < 0.01$, $***p < 0.001$ and $****p < 0.0001$.

Results and discussion

CpE phytochemical screening

Figure 3 shows CpE prepared by percolation method. The qualitative phytochemical screening of CpE was found to contain alkaloids, flavonoids, terpenoids, phenols and tannins. Kar et al. (2018) and Morsy et al. (2016) have also reported the presence of those natural products in extract of *Calotropis procera* (Morsy et al. 2016; Kar et al. 2018). These phytochemicals have potent anti-cancer activities, but encapsulation of those phenolic compounds can aid their anti-cancer properties and safe delivery in complex human body (Huang et al. 2010; Samy et al. 2012a).

Emulsion dispersity analysis

For water in oil monodisperse microemulsion, the flow rate for the continuous phase was adjusted to 4.26 mL/h and for the dispersed phase was adjusted to 1.80 mL/h. The water in oil emulsion provides a chemical reaction to occur within the aqueous phase and acts as microreactor for nanoparticles synthesis. The factors, such as size and shape of

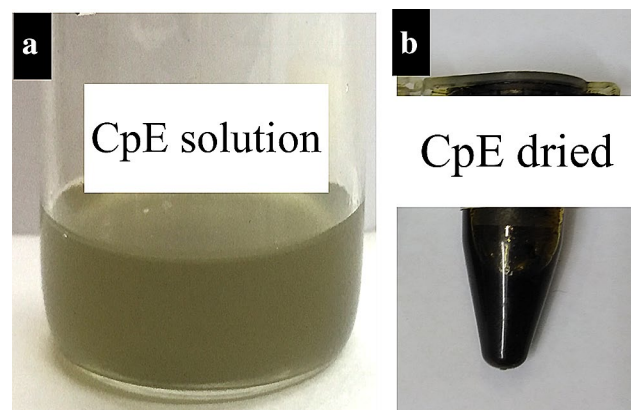


Fig. 3 *Calotropis procera* extract (CpE): **a** hydro-alcoholic (ethanol + d. H_2O) CpE solution. **b** The sticky blackish green colour (CpE)

microemulsions, influence the mixing speed and reaction in aqueous phase. The spherical and monodispersed microemulsions provide uniform distribution of microenvironment to a reaction mixture which ultimately contributes significantly in the formation of high-encapsulation efficiency drug carriers (Damiati et al. 2018). Therefore, the monodispersed emulsions ($0.49 \text{ mm} \pm 0.02$) formed in this research by microfluidic system were proposed to provide microcarriers with uniform size distribution and high-encapsulation efficiency of CpE.

Characterization of CpE–CsAg microcarriers

UV-spectrum analysis

The samples collected from microchip at $95 \text{ }^\circ\text{C}$ did not show any change in colour. However, with the addition of 10% NaOH, the colour changed from light green to reddish brown. This change in colour was quite visible after every 30 s; however, the reddish brown colour became stable after 90 s and no change was observed afterwards (Fig. 4). The change in colour and the intensity of reddish brown colour is due to the excitation of AgNO_3 surface plasmon resonance, confirming the formation of silver nanoparticles (Kalaivani et al. 2018). The UV–Vis spectrum of samples without NaOH had not shown the silver nanoparticle characteristic peak around 400 nm and peak of CpE was quite visible at 340 nm (Electronic supplementary material figure ESM_1). This indicates that CpE was unable to reduce AgNO_3 and NaOH was required as reducing agent for synthesis of CsAg. This might be because of the difference in the preparation of plant extract in the current research as compared to the

earlier reported studies in which the leaves of *Calotropis procera* were just cut, boiled and filtered and the filtrate was then used for reduction of silver nanoparticles (Dada et al. 2017; Mutluq Alkammash 2017). Although, in this research, the proficient maceration and percolation methods had been used for the extraction of pharmacological active phytochemicals as described in Sect. 2.2.

It was observed that there was no peak of silver nanoparticles in UV–Vis spectrum when analysis was performed at room temperature as shown in Fig. 5a. This is because precipitates of Ag_2O were formed after 30–40 min by adding NaOH. Therefore, it was inferred that in order to obtain the adequate capping property of chitosan for stabilization of silver nanoparticles, the chitosan is needed to be heated up to $95 \text{ }^\circ\text{C}$. After heating the reaction mixture at $95 \text{ }^\circ\text{C}$, the resulting CsAg were found to be more stable and had shown quite visible peak around 400 nm as indicated in Fig. 5b. These results justified that the chitosan capping ability increases as it is heated to $95 \text{ }^\circ\text{C}$ which is in agreement with the previous reported studies (Akmaz et al. 2013; Nate et al. 2018). In UV–Vis spectrometry of CpE, a wide peak at 340 nm corresponds to the unsaturated groups (Jain et al. 2016). This peak was observed in every sample of CsAg which is justifying the encapsulation of CpE in microspheres. The fluctuation in the temperature of water bath was noticed to be $95 \pm 5 \text{ }^\circ\text{C}$.

SEM analysis and %EE calculation

The samples prepared at room temperature had revealed the flower-like appearance consisting of interconnected nano-needles of Ag_2O with mean diameter of $161 \pm 25 \text{ nm}$ as shown in (ESM_2). These results were in agreement

Fig. 4 The change in colour of CpE–CsAg with the time after adding 10% NaOH

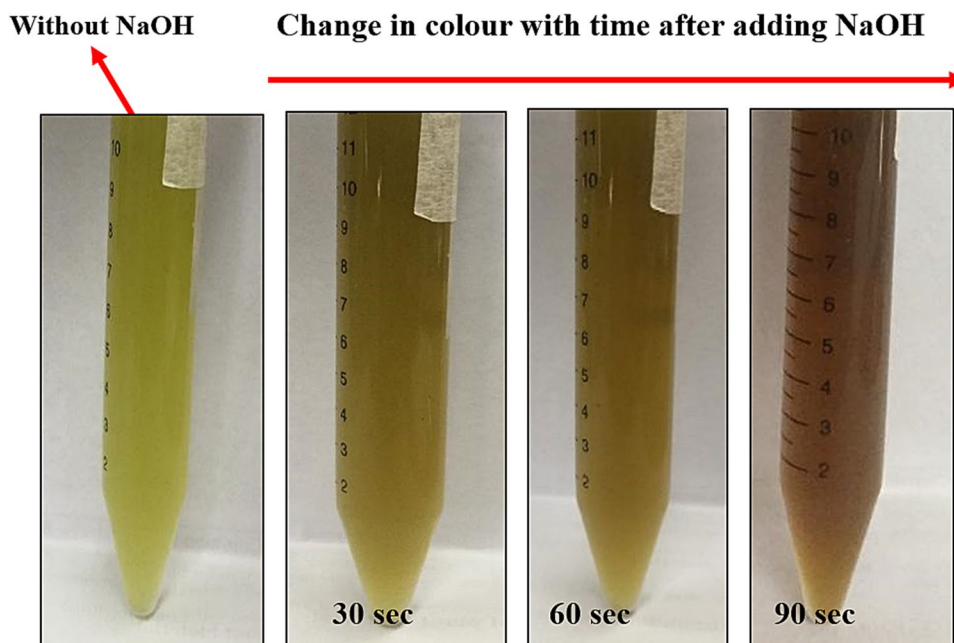
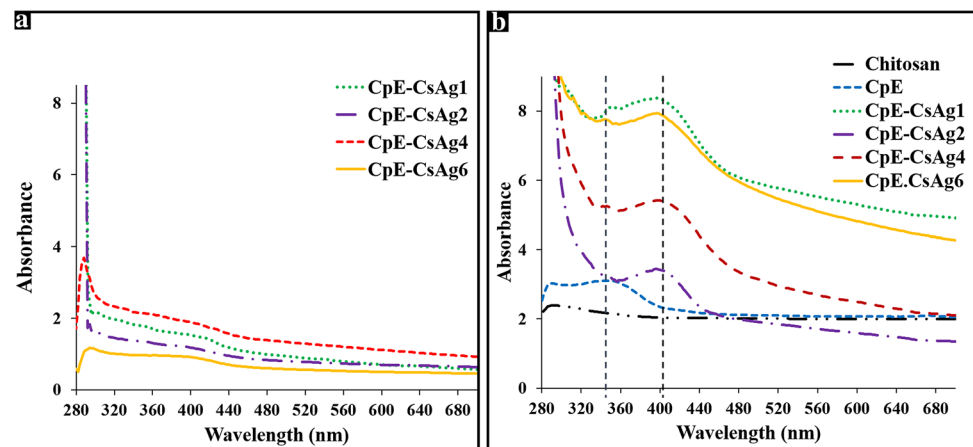


Fig. 5 UV–Vis spectrum of CsAg microcarriers encapsulating CpE. **a** The UV–vis graph of samples obtained without heating. **b** UV–vis graph of samples obtained with heating. Samples CpE–CsAg 1, 2, 4 and 6 = the volumetric ratio of CpE added in 4:1 of chitosan: AgNO₃



with the literature (Wei et al. 2011; Zhou et al. 2014). The SEM image confirmed that the silver nanoparticles were not formed at room temperature as justified by the absence of characteristic peak of silver in UV–Vis graph.

Figure 6 illustrates the SEM images of microcarriers and silver nanoparticles synthesized at 95 °C using PTFE tubular reactor. The SEM analysis of chitosan raw powder revealed its non-porous and smooth surface which was similar to the CpE surface morphology with only difference of cake-like appearance of chitosan as shown in Fig. 6a, b, respectively. The unloaded CsAg revealed the irregular shaped particles with rough surface morphology which might be due to some agglomeration of silver particles. While on loading the CpE in CsAg, a significantly different morphology of microcarriers was noticed. The spherical silver nanoparticles became quite visible on smooth surface of chitosan and CpE at magnification scale of 5 μm and 10 μm shown in Fig. 6c–g. It can be interpreted that CpE might also play a role in the surface morphology and stability of silver nanoparticles to some extent. Therefore, the difference in size of silver nanoparticles in different samples is significant and can be related to the role of drug in stabilization of particles. In this research, smooth circular chitosan microspheres were also visible with size distribution of $23.7 \pm 14 \mu\text{m}$ at a magnification of 200 μm . Therefore, this could be claimed that silver nanoparticles were found embedded in chitosan microspheres.

The CpE–CsAg microcarriers formed by heating were found to have higher % EE (average 77.125%) as compared to the ones found for non-heated samples (average % EE = 57.195%). The difference in % EE may be due to the role of CsAg microcarriers which appears as significant encapsulating agent for drug as compared to the Ag₂O nano-needles. It was also found that the CsAg loaded with CpE of volumetric ratio 2 showed adequate % EE (77.25%) with even sized distribution of silver nanoparticles ($97.5 \pm 8.8 \text{ nm}$). The SEM images and high % EE are

confirming the significant role of monodispersed microemulsions in the formation of evenly sized distributed chitosan microcarriers embedding the silver nanoparticles and CpE.

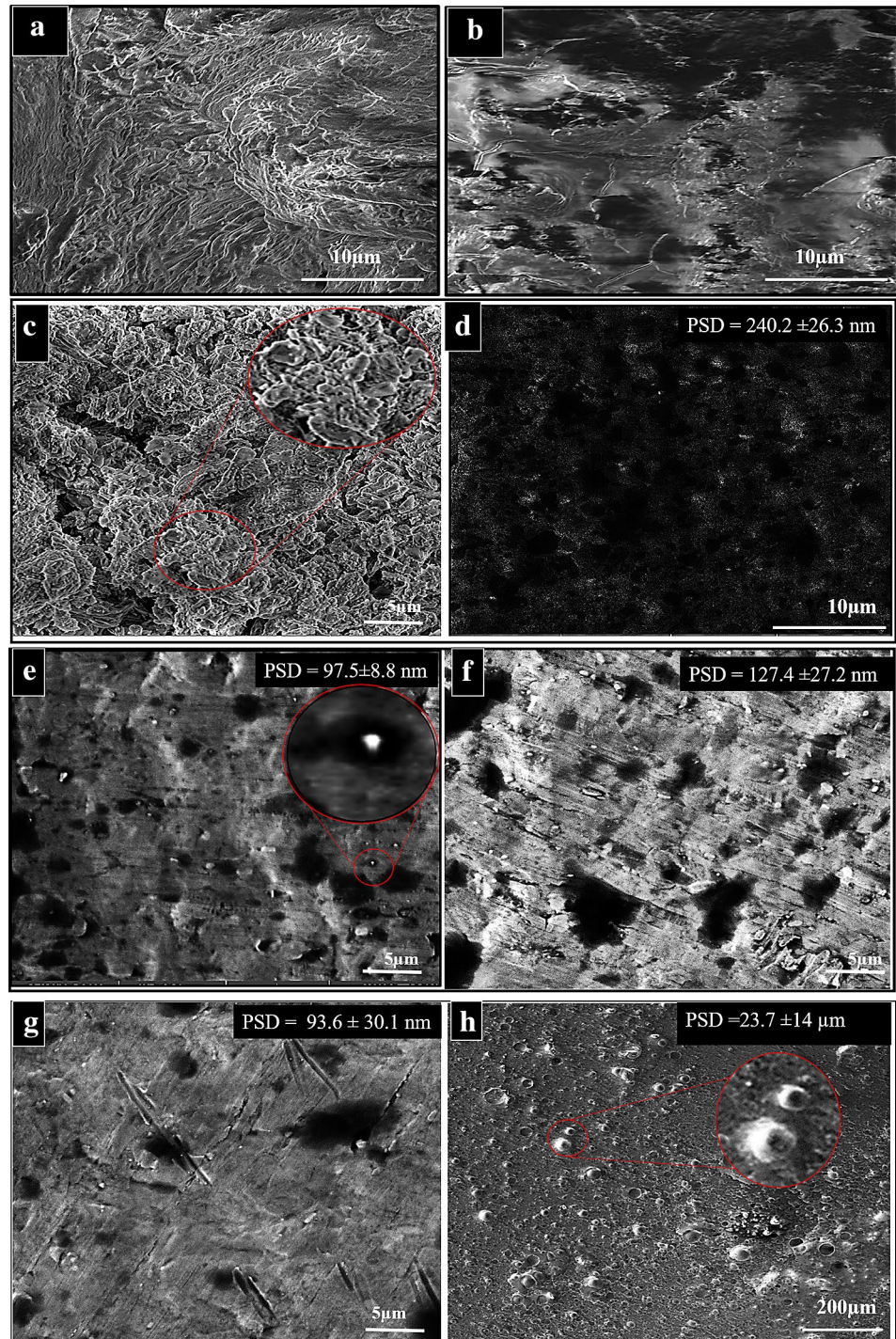
The silver nanoparticles shows an optical absorption typical band peak for metallic silver nano-crystallites (Murugan et al. 2016) as evident by the EDX results (Fig. 7a). The Fe peak might be due to its presence in CpE (Verma 2014) and the peaks of oxygen and carbon were due to polymeric chitosan layer on stable silver nanoparticles. The peak of Al came from the substrate used to analyze the EDX of sample. Along with the qualitative analysis, the quantitative measurement in % weight was also performed for silver nanoparticles (4.9%) as shown in Fig. 7b. EDX analysis confirmed the presence of silver nanoparticles in the sample capped with polymeric chitosan with no evidence for Ag₂O (Murugan et al. 2016; Yang et al. 2016).

FTIR analysis confirming the CpE–CsAg microcarriers formation

The absorbance of IR by various functional groups of CpE and CsAg microcarriers is given in Table 1 and spectrum is illustrated in Fig. 8. The CpE displayed the peaks at various intensities which represents the presence of multifaceted functional groups. The absorbance at 1304 cm^{-1} , 1277 cm^{-1} and 1043 cm^{-1} confirming the presence of primary and secondary alcohols, flavonoids and tertiary alcohol, respectively (Oliveira et al. 2016). The FTIR peaks verified the phytochemicals screening results for the presence of phenols and flavonoids. Furthermore, the appearance of CpE functional groups in CpE–CsAg microcarriers indicated the successful encapsulation of CpE in CsAg.

The shifting and disappearance of chitosan peaks in CsAg and control samples were noticeable that might be due to the formation of composites as reported earlier (Govindan et al. 2012). The peak of chitosan seen at wavelength 1636 cm^{-1} indicated the amino group of amide bonds which confirmed presence of acetyl group of deacetylated chitin and chitosan

Fig. 6 The SEM images **a** chitosan powder, **b** CpE, **c** CsAg microcarriers without CpE, **d** CpE–CsAg1, **e** CpE–CsAg2, **f** CpE–CsAg4, **g** CpE–CsAg6 and **h** the magnification scale of 200 μm showing spherical chitosan microspheres embedding the silver nanoparticles



–CONH₂ bond (Venkatesham et al. 2014). The disappearance of chitosan peak at 1636 cm^{-1} and appearance of small band of *N*-acetyl group (amide II) at 1557 cm^{-1} justified the stabilization of silver nanoparticles by chitosan amino groups (Queiroz et al. 2015). Furthermore, the slight broadening and elevation of peak around 3280 cm^{-1} in CsAg and control samples indicated the role of amino and hydroxyl groups of chitosan in chelation and stabilization of silver

ions (Chen et al. 2014; Kalaivani et al. 2018; Nate et al. 2018).

Anti-oxidant activity

H₂O₂ is sometimes toxic to the cells since it gives rise to high concentration of hydroxyl radicals. Therefore, the anti-oxidant activity of extract and microcarriers can

Fig. 7 The SEM–EDX of CpE–CsAg microcarriers **a** the qualitative analysis for the presence of silver in microcarriers. **b** The quantitative weight % of different components present in the microcarriers. The yellow circles indicate the site of Ag on graph

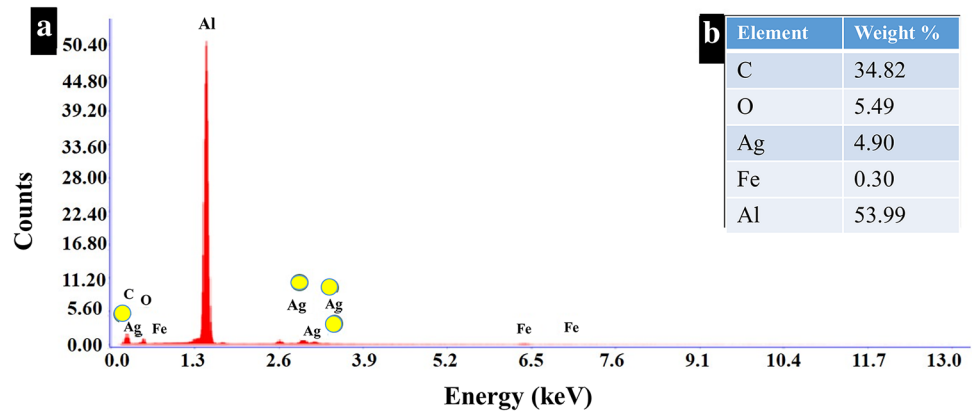


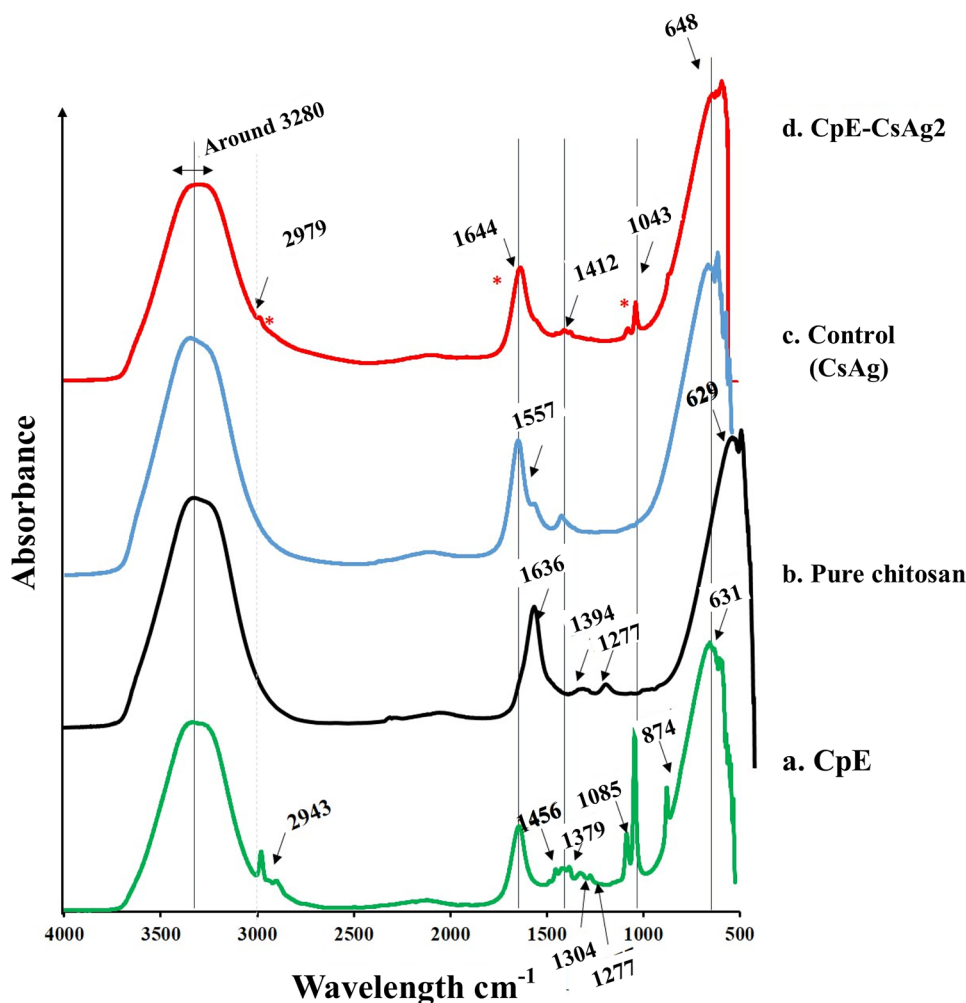
Table 1 The FTIR peak analysis of CpE and CpE–CsAg microcarriers

Peaks at wavelength (cm ⁻¹)	Present in samples	Functional group and vibrational mode	Compound classification
Around 3280	All	–OH and NH ₂ group (NH-amine group),	Which indicates the polysaccharide or polymeric –OH stretch (Chen et al. 2014; Venkatesham et al. 2014; Queiroz et al. 2015)
2979	CpE, CsAg and CpE–CsAg microcarriers	C–H asymmetric stretch	Aliphatic compounds (Palem et al. 2018)
2943	CpE	C–H symmetric stretching	aliphatic compounds (Chen et al. 2014; Queiroz et al. 2015)
1644	CpE, CsAg and CpE–CsAg microcarriers	Secondary amide stretch C–O	Amide I (Govindan et al. 2012; Queiroz et al. 2015; Palem et al. 2018)
1636	Pure Chitosan	Secondary amide stretch C–O	Amide I (Govindan et al. 2012; Queiroz et al. 2015; Palem et al. 2018)
1546	In both CsAg	N–H bending	Amide II (Queiroz et al. 2015)
1456–1379	CpE	CH ₂ bending and CH ₃ symmetric bending	
1412	CpE, CsAg and CpE–CsAg microcarriers	CH ₂ bending and CH ₃ deformation (Queiroz et al. 2015; Palem et al. 2018)	
1394	Pure chitosan	CH ₃ symmetrical deformation (Queiroz et al. 2015)	
1304	CpE	CH ₂ OH and –CHROH	Primary and secondary alcohols (Oliveira et al. 2016)
1277	CpE and Pure Chitosan	C–O, a carboxyl group	Polyols such as flavonoids (Oliveira et al. 2016)
1085	CpE, CsAg and CpE–CsAg microcarriers	C–O–C	Dimethyl ethers (Oliveira et al. 2016)
1043	CpE, CsAg and CpE–CsAg microcarriers	C–O and –OH deformation (–CR ₂ OH)	Tertiary alcohols (Oliveira et al. 2016)
874	CpE, CsAg and CpE–CsAg microcarriers	–CH ring stretching	Monosaccharides (Oliveira et al. 2016)

be evaluated by H₂O₂ anti-oxidant assay. The research results indicated that the H₂O₂ scavenging ability of CpE and CpE–CsAg₂ were dependent on their concentration as shown in Fig. 9. The scavenging ability of loaded microcarriers (CpE–CsAg₂, IC₅₀ = 88.78 ± 15 µg/mL) was found to be higher as compared to the CpE (IC₅₀ = 110.4 ± 18 µg/mL) at low concentration. The highest anti-oxidant activity of CpE was 71% which was similar to the previous reports (Rani et al. 2018). The radical scavenging ability of CpE and CpE–CsAg₂ was

significantly different (*p* < 0.01) from ascorbic acid. These results confirmed that the CsAg microcarriers play a vital role in increasing the radical scavenging proficiency of CpE. Hence, CpE-loaded CsAg microcarriers were predicted to have powerful combinational effect in anti-breast cancer activity by arresting the high-level reactive oxygen species (ROS). After validation of H₂O₂ scavenging ability, the loaded microcarriers were evaluated for their anti-tumour activity.

Fig. 8 The FTIR spectra of **a** CpE, **b** chitosan powder, **c** control containing only the CsAg microcarriers, **d** CpE–CsAg2 microcarriers (chitosan:AgNO₃:CpE; 4:1:2). Red asterisk * representing the peak of CpE



In vitro anti-breast cancer activity

The aforementioned analysis confirmed that the CpE had been successfully encapsulated into CsAg microcarriers. Therefore, it could be easily utilized to achieve a combinational therapy approach to halt the growth of breast cancer cells. Figure 10 demonstrates that the CsAg microspheres enhanced the cytotoxicity of CpE significantly, that is stronger than CpE alone. After 24 h of incubation, CpE reduced 9% of cells viability at concentration of 80 $\mu\text{g}/\text{mL}$, while CpE.CsAg6 could reduce 52.33% cells viability at concentration of 100 $\mu\text{g}/\text{mL}$. Moreover, CpE–CsAg2 showed the most significant anti-cancer cytotoxicity with reduced cells viability up to 6.34% and 4.63% at concentrations of 80 $\mu\text{g}/\text{mL}$ and 100 $\mu\text{g}/\text{mL}$ respectively. These results confirmed that the CpE-loaded CsAg microcarriers could effectively kill the 4T1 breast cancer cells on concentration-dependent manner. When the concentration of CpE–CsAg2 was more than 80 $\mu\text{g}/\text{mL}$, it could inhibit the growth of cancer cells above 95%.

The IC₅₀ values were measured to quantitatively characterize the cytotoxicity of CpE and CpE–CsAg2 in order to estimate the concentration of drug required for 50% of cell death. The IC₅₀ value of CpE–CsAg2 was 42.53 $\mu\text{g}/\text{mL}$ which was much lower than the values obtained for CpE (~60.54 $\mu\text{g}/\text{mL}$). The increased cytotoxicity of CpE-loaded CsAg against the 4T1 cells might be because of improvement in endocytosis uptake of the drug due to chitosan microcarriers which eventually increases the intracellular CpE concentration and leads to cell death.

Previously, CpE has been reported to show significant results in suppressing the growth of tumour cells (Alzaharani et al. 2017). The root extract of *Calotropis procera* has known to contain biological active protein that matches apolipoprotein A-I protein which acts in the suppression of breast cancer via the NF- κ B pathway (Samy et al. 2012b). Likewise, chitosan and silver composites anti-breast cancer activity has been very well characterized in the previous reported studies (Nayak et al. 2016; Abaza et al. 2018; Bilal et al. 2019). However, the capability of CpE-loaded

Dunnett's multiple comparisons test	P values	Significant?	Summary
Ascorbic Acid vs. CpE	<0.01	Yes	**
Ascorbic Acid vs. CpE2	<0.01	Yes	**

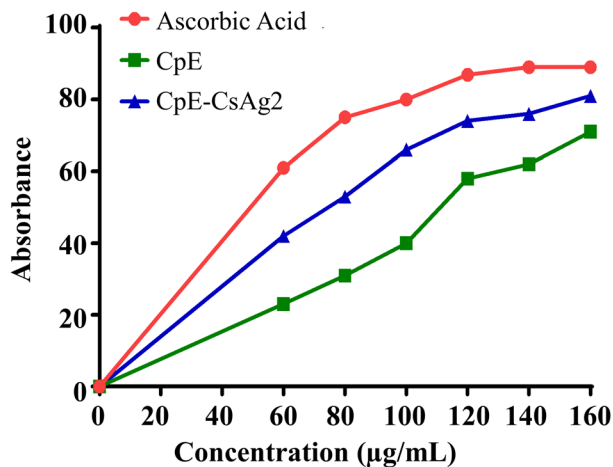


Fig. 9 The H₂O₂ radical scavenging activity graph. Comparing the anti-oxidant activity of CpE and CpE–CsAg₂. The table above demonstrate the significance of CpE–CsAg₂ evaluated by Dunnnett’s multiple comparisons test. Every value represents the mean (*n*=3) and ***p*<0.01

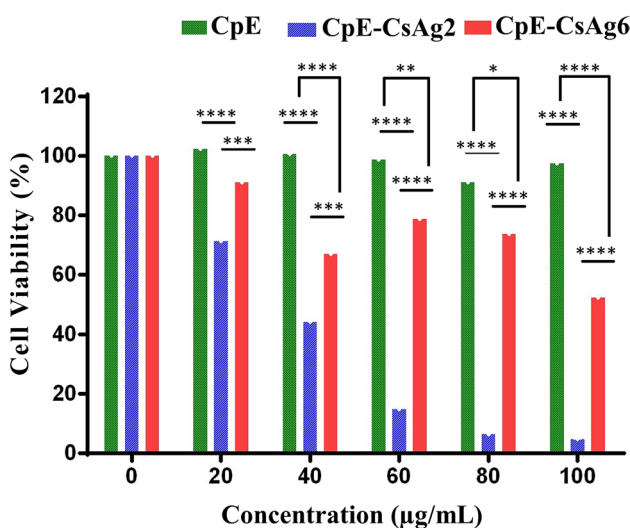


Fig. 10 In vitro cytotoxicity of CpE, CpE–CsAg₂ and CpE–CsAg₆ against 4T1 cells by MTT assay. Each value represents the mean (*n*=8). Statistical analysis was performed using ANOVA followed by Tukey’s multiple comparison test (**p*<0.5, ***p*<0.01, ****p*<0.001 and *****p*<0.0001) which is evaluating the results as highly significant

CsAg microcarriers synthesized in this research to inhibit the breast cancer proliferation with above 95% efficacy has not been reported previously.

Conclusion

In this research, the CsAg composites were synthesized as microcarriers for encapsulation of CpE to increase its bioavailability. The microcarriers synthesized at room temperature in microchip were found to precipitate out as Ag₂O because of the instability of silver nanoparticles. On the other hand, stabilized silver nanoparticles were formed upon heating the reaction mixture at 95 °C in PTFE microfluidic reactor. These results showed the effect of heating on chitosan as an essential parameter to act as an efficient stabilizing agent. The characterization of these microcarriers had justified the formation of CsAg microcarriers and encapsulation of CpE with high % EE 77.125 ± 6.9%. Microfluidic system was found to be an efficient method for one-step encapsulation of anti-oxidant with uniform sized distribution of particles. Moreover, these loaded microcarriers had shown a remarkable activity to inhibit the 4T1 cell proliferation (*p*<0.0001). This work has emphasized on the combinational therapeutic applications of microfluidic system. It can also be concluded that the lack of any noticeable toxicity of CsAg provides safe application of these microspheres in anti-cancer therapy. The in vivo studies in future can further validate the synergistic combination of CpE, chitosan and silver to suppress the breast cancer cell growth.

Acknowledgements This research is supported by Pakistan Institute of Engineering and Applied Sciences (PIEAS), Islamabad, Pakistan. Authors are grateful to Mr. Asghar Ali and Mr. Islam Khattak for providing technical support in various stages of research. We extend our heartfelt thanks to Engr. Usman Aftab for his significant assistance in proofreading of this research. We are also thankful to Malik Ihsanullah Khan from Division of Molecular Medicine (USTC) for helping in preparation of plant extract and its phytochemical analysis. The authors would like to pay a special thanks to University of Science and Technology of China for providing chitosan (CAS: 9012-76-4, Sigma).

Compliance with ethical standards

Conflict of interest There are no conflicts to declare.

References

Abaza A, Mahmoud GA, Hegazy EA et al (2018) Cytotoxic effect of chitosan based nanocomposite synthesized by radiation: in vitro liver and breast cancer cell line. *J Pharm Pharmacol*. <https://doi.org/10.17265/2328-2150/2018.04.002>

Adhikari HS, Yadav PN (2018) Anticancer activity of chitosan, chitosan derivatives, and their mechanism of action. *Int J Biomater* 2018:1–29. <https://doi.org/10.1155/2018/2952085>

Akmaz S, Dilaver Adgüzel E, Yasar M, Erguven O (2013) The effect of ag content of the chitosan-silver nanoparticle composite material on the structure and antibacterial activity. *Adv Mater Sci Eng* 2013:6. <https://doi.org/10.1155/2013/690918>

- Alzahrani HS, Swed Alzahrani H, Mutwakil M et al (2017) Anticancer and antibacterial activity of *Calotropis procera* leaf extract. J Basic Appl Sci Res 7:18–25
- Alzahrani HS, Almalki SA, Rizgallah MR (2019) Study of the cytotoxic effect of *Calotropis procera* on breast cancer cell line T47D in vitro: a traditional remedy. Int J Sci Innov 7:107–112. <https://doi.org/10.32594/IJSI>
- American Cancer Society (2019) Cancer facts & figures 2019: Atlanta. Am cancer Soc 1–76
- Amoyav B, Benny O (2018) Controlled and tunable polymer particles' production using a single microfluidic device. Appl Nanosci 8:905–914. <https://doi.org/10.1007/s13204-018-0790-0>
- Bilal M, Zhao Y, Rasheed T et al (2019) Biogenic nanoparticle–chitosan conjugates with antimicrobial, antibiofilm, and anticancer potentialities: development and characterization. Int J Environ Res Public Health 16:598–612. <https://doi.org/10.3390/ijerph16040598>
- Chandirika JU, Sindhu R, Selvakumar S, Annadurai G (2018) Herbal extract encapsulated in chitosan nanoparticles: a novel strategy for the treatment of urolithiasis. INDO Am J Pharm Sci 1:1955–1961. <https://doi.org/10.5281/zenodo.1212445>
- Chen Q, Jiang H, Ye H et al (2014) Preparation, antibacterial, and antioxidant activities of silver/chitosan composites. J Carbohydr Chem 33:298–312. <https://doi.org/10.1080/07328303.2014.931962>
- Dada AO, Ojediran OJ, Dada FE et al (2017) Green synthesis and characterization of silver nanoparticles using *Calotropis procera* extract. Orig Res Artic J Appl Chem Sci Int 8:137–143
- Damiati S, Kompella UB, Damiati SA, Kodzius R (2018) Microfluidic devices for drug delivery systems and drug screening. Genes (Basel) 9:103. <https://doi.org/10.3390/genes9020103>
- Ellahi R, Hussain F, Asad Abbas S et al (2020) Study of two-phase newtonian nanofluid flow hybrid with hafnium particles under the effects of slip. Inventions 5:6. <https://doi.org/10.3390/inventions5010006>
- Farouk AEA, Ahamed NT, Alzahrani O et al (2016) Antimicrobial activities evaluation from the extracts of leaves, flowers, fruits and latex of *calotropis procera* from Taif. Int J Curr Microbiol Appl Sci 5:240–256. <https://doi.org/10.20546/ijemas.2016.511.026>
- Govindan S, Nivethaa EAK, Saravanan R et al (2012) Synthesis and characterization of chitosan–silver nanocomposite. Appl Nanosci. <https://doi.org/10.1007/s13204-012-0109-5>
- Gul R, Jan SU, Faridullah S et al (2017) Preliminary phytochemical screening, quantitative analysis of alkaloids, and antioxidant activity of crude plant extracts from *ephedra intermedia* indigenous to balochistan. Sci World J. <https://doi.org/10.1155/2017/5873648>
- Hintzer K, Zipplies T, Carlson DP, Schmiegel W (2016) Fluoropolymers, organic. Ullmann's encyclopedia of industrial chemistry. Wiley-VCH Verlag GmbH & Co. KGaA, Weinheim, pp 1–55
- Hoseinzadeh S, Ramezani AH (2019) Investigation of Ta/NiI-WO₃ /FTO structures as a semiconductor for the future of nanodevices. J Nanoelectron Optoelectron 14:1413–1419. <https://doi.org/10.1166/jno.2019.2564>
- Hoseinzadeh S, Ghasemiasl R, Bahari A, Ramezani AH (2017a) n-type WO₃ semiconductor as a cathode electrochromic material for ECD devices. J Mater Sci Mater Electron 28:14446–14452. <https://doi.org/10.1007/s10854-017-7306-7>
- Hoseinzadeh S, Ghasemiasl R, Bahari A, Ramezani AH (2017b) The injection of Ag nanoparticles on surface of WO₃ thin film: enhanced electrochromic coloration efficiency and switching response. J Mater Sci Mater Electron 28:14855–14863. <https://doi.org/10.1007/s10854-017-7357-9>
- Hoseinzadeh S, Ghasemiasl R, Bahari A, Ramezani AH (2018) Effect of post-annealing on the electrochromic properties of layer-by-layer arrangement FTO-WO₃-Ag-WO₃-Ag. J Electron Mater 47:3552–3559. <https://doi.org/10.1007/s11664-018-6199-4>
- Huang WY, Cai YZ, Zhang Y (2010) Natural phenolic compounds from medicinal herbs and dietary plants: potential use for cancer prevention. Nutr Cancer 62:1–20. <https://doi.org/10.1080/01635580903191585>
- Hussein-Al-Ali SH, Kura A, Hussein MZ, Fakurazi S (2018) Preparation of chitosan nanoparticles as a drug delivery system for perindopril erbumine. Polym Compos 39:544–552. <https://doi.org/10.1002/pc.23967>
- Jacob S, Nair AB, Shah J (2020) Emerging role of nanosuspensions in drug delivery systems. Biomater Res 24
- Jain PK, Soni A, Jain P, Bhawsar J (2016) Phytochemical analysis of *Mentha spicata* plant extract using UV–VIS, FTIR and GC/MS technique. J Chem Pharm Res 8:1–6
- Kalaivani R, Maruthupandy M, Muneeswaran T et al (2018) Synthesis of chitosan mediated silver nanoparticles (Ag NPs) for potential antimicrobial applications. Front Lab Med 2:30–35. <https://doi.org/10.1016/j.flm.2018.04.002>
- Kar D, Pattnaik PK, Pattnaik B, Kuanar A (2018) Antimicrobial analysis of different parts extract in different solvent system of a waste weed-*Calotropis procera*. Asian J Pharm Clin Res 11:227–231. <https://doi.org/10.22159/ajpcr.2018.v11i2.21081>
- Kaur H (2018) Review on the extraction methods used in medicinal plants. Int J Adv Manag Technol Eng Sci
- Kesente M, Kavetsou E, Roussaki M et al (2017) Encapsulation of olive leaves extracts in biodegradable PLA nanoparticles for use in cosmetic formulation. Bioengineering 4:1–14. <https://doi.org/10.3390/bioengineering4030075>
- Khanzada SK, Shaikh W, Kazi TG et al (2008) Analysis of fatty acid, elemental and total protein of *Calotropis procera* medicinal plant from Sindh, Pakistan. Pakistan J Bot 40:1913–1921
- Kong T, Wu J, Yeung KWK et al (2013) Microfluidic fabrication of polymeric core–shell microspheres for controlled release applications. Biomicrofluidics. <https://doi.org/10.1063/1.4819274>
- Kumhari SVKR, Kummara MR, Palem RR et al (2015) Chitosan-poly(aminopropyl)phenylsilsequioxane hybrid nanocomposite membranes for antibacterial and drug delivery applications. Polym Int 64:293–302. <https://doi.org/10.1002/pi.4789>
- Li J, Cai C, Li J et al (2018) Chitosan-based nanomaterials for drug delivery. Molecules 23:1–26. <https://doi.org/10.3390/molecules23102661>
- Maslanka Figueroa S, Fleischmann D, Beck S, Goepferich A (2020) Thermodynamic, spatial and methodological considerations for the manufacturing of therapeutic polymer nanoparticles. Pharm Res 37:59. <https://doi.org/10.1007/s11095-020-2783-4>
- Medina-Sánchez M, Xu H, Schmidt OG (2018) Micro- and nanomotors: the new generation of drug carriers. Ther Deliv 9:303–316. <https://doi.org/10.4155/tde-2017-0113>
- Mohan CO, Gunasekaran S, Ravishankar CN (2019) Chitosan-capped gold nanoparticles for indicating temperature abuse in frozen stored products. NPJ Sci Food 3:2. <https://doi.org/10.1038/s41538-019-0034-z>
- Morsy N, Al Sherif EA, Abdel-Rassol TMA (2016) Phytochemical analysis of *Calotropis procera* with antimicrobial activity investigation. Main Gr Chem 15:267–273. <https://doi.org/10.3233/MGC-160206>
- Munin A, Edwards-Lévy F (2011) Encapsulation of natural polyphenolic compounds; a review. Pharmaceutics 3:793–829. <https://doi.org/10.3390/pharmaceutics3040793>
- Murugan K, Anitha J, Dinesh D et al (2016) Fabrication of nano-mosquitocides using chitosan from crab shells: Impact on non-target organisms in the aquatic environment. Ecotoxicol Environ Saf 132:318–328. <https://doi.org/10.1016/j.ecoenv.2016.06.021>
- Mutluq Alkammash N (2017) Synthesis of silver nanoparticles from artemisia sieberiana and *calotropis procera* medical plant extracts and their characterization using SEM analysis. Biosci Biotechnol Res Asia 14:521–526. <https://doi.org/10.13005/bbra/2474>

- Nair R, Reddy BH, Kumar CKA, Kumar KJ (2009) Application of chitosan microspheres as drug carriers: a review. *J Pharm Sci Res* 1:1–12
- Najafi-Ashtiani H, Bahari A, Gholipour S, Hoseinzadeh S (2018) Structural, optical and electrical properties of WO₃–Ag nanocomposites for the electro-optical devices. *Appl Phys A Mater Sci Process* 124:1–9. <https://doi.org/10.1007/s00339-017-1412-5>
- Nate Z, Moloto MJ, Mubiayi PK, Sibiya PN (2018) Green synthesis of chitosan capped silver nanoparticles and their antimicrobial activity. *MRS Adv* 3:2505–2517. <https://doi.org/10.1557/adv.2018.368>
- Nayak D, Minz AP, Ashe S et al (2016) Synergistic combination of antioxidants, silver nanoparticles and chitosan in a nanoparticle based formulation: characterization and cytotoxic effect on MCF-7 breast cancer cell lines. *J Colloid Interface Sci* 470:142–152. <https://doi.org/10.1016/j.jcis.2016.02.043>
- Obayemi JD, Soboyejo WO, Odusanya OS, et al (2014) Abstract B40: Injectable multifunctional biodegradable polymeric microspheres for localized drug delivery in breast cancer treatment. In: *Cancer Epidemiology and Prevention Biomarkers*. American Association for Cancer Research (AACR), pp B40–B40
- Oliveira RN, Mancini MC, de Oliveira FCS et al (2016) FTIR analysis and quantification of phenols and flavonoids of five commercially available plants extracts used in wound healing. *Matéria (Rio Janeiro)* 21:767–779. <https://doi.org/10.1590/s1517-707620160003.0072>
- Palem RR, Saha N, Shimoga GD et al (2018) Chitosan–silver nanocomposites: new functional biomaterial for health-care applications. *Int J Polym Mater Polym Biomater* 67:1–10. <https://doi.org/10.1080/00914037.2017.1291516>
- Queiroz MF, Melo KRT, Sabry DA et al (2015) Does the use of chitosan contribute to oxalate kidney stone formation? *Mar Drugs* 13:141–158. <https://doi.org/10.3390/md13010141>
- Rani R, Sharma D, Chaturvedi M, Yadav JP (2018) Phytochemical analysis, antibacterial and antioxidant activity of *Calotropis procera* and *Calotropis gigantea*. *Nat Prod J*. <https://doi.org/10.2174/2210315508666180608081407>
- Ruch RJ, Cheng SJ, Klaunig JE (1989) Prevention of cytotoxicity and inhibition of intercellular communication by antioxidant catechins isolated from chinese green tea. *Carcinogenesis* 10:1003–1008. <https://doi.org/10.1093/carcin/10.6.1003>
- Salari E, Peyghambarzadeh SM, Sarafraz MM, Hormozi F (2016) Boiling thermal performance of TiO₂ aqueous nanofluids as a coolant on a disc copper block. *Period Polytech Chem Eng* 60:106–122. <https://doi.org/10.3311/ppch.8262>
- Salari E, Peyghambarzadeh SM, Sarafraz MM et al (2017) Thermal behavior of aqueous iron oxide nano-fluid as a coolant on a flat disc heater under the pool boiling condition. *Heat Mass Transf und Stoffuebertragung* 53:265–275. <https://doi.org/10.1007/s00231-016-1823-4>
- Samy RP, Rajendran P, Li F et al (2012a) Identification of a novel *Calotropis procera* protein that can suppress tumor growth in breast cancer through the suppression of NF-κB pathway. *PLoS ONE* 7:1–14. <https://doi.org/10.1371/journal.pone.0048514>
- Samy RP, Rajendran P, Li F et al (2012b) Identification of a novel *Calotropis procera* protein that can suppress tumor growth in breast cancer through the suppression of NF-κB pathway. *PLoS ONE*. <https://doi.org/10.1371/journal.pone.0048514>
- Sarafraz MM, Arjomandi M (2018a) Demonstration of plausible application of gallium nano-suspension in microchannel solar thermal receiver: experimental assessment of thermo-hydraulic performance of microchannel. *Int Commun Heat Mass Transf* 94:39–46. <https://doi.org/10.1016/j.icheatmasstransfer.2018.03.013>
- Sarafraz MM, Arjomandi M (2018b) Thermal performance analysis of a microchannel heat sink cooling with copper oxide-indium (CuO/In) nano-suspensions at high-temperatures. *Appl Therm Eng* 137:700–709. <https://doi.org/10.1016/j.applthermaleng.2018.04.024>
- Sarafraz MM, Hormozi F, Kamalgharibi M (2014) Sedimentation and convective boiling heat transfer of CuO–water/ethylene glycol nanofluids. *Heat Mass Transf und Stoffuebertragung* 50:1237–1249. <https://doi.org/10.1007/s00231-014-1336-y>
- Shahzadi I, Bashir M, Bashir S, Inayat MH (2018) Thermally assisted coating of PVA for hydrophilic surface modification of PMMA microchannel for oil in water emulsion. In: *Proceedings of 2018 15th International Bhurban Conference on Applied Sciences and Technology, IBCAST 2018*. pp 51–54
- Singh M, Sinha I, Mandal RK (2009) Role of pH in the green synthesis of silver nanoparticles. *Mater Lett* 63:425–427. <https://doi.org/10.1016/j.matlet.2008.10.067>
- Stoica R, Şomoghi R, Ion RM (2013) Preparation of chitosan–tripolyphosphate nanoparticles for the encapsulation of polyphenols extracted from rose hips. *Dig J Nanomater Biostruct* 8:955–963
- Tsao CW, DeVoe DL (2009) Bonding of thermoplastic polymer microfluidics. *Microfluid Nanofluidics* 6:1–6. <https://doi.org/10.1007/s10404-008-0361-x>
- Van Phu D, Duy NN, Quoc LA, Hien NQ (2009) The effect of pH and molecular weight of chitosan on silver nanoparticles synthesized by irradiation. *Res Dev Cent Radiat Technol* 47:47–52
- Venkatesham M, Ayodhya D, Madhusudhan A et al (2014) A novel green one-step synthesis of silver nanoparticles using chitosan: catalytic activity and antimicrobial studies. *Appl Nanosci*. <https://doi.org/10.1007/s13204-012-0180-y>
- Verma VN (2014) The chemical study of calotropis. *Int Lett Chem Phys Astron* 1:74–90. <https://doi.org/10.18052/www.scipress.com/ILCPA.20.74>
- Vimala K, Mohan YM, Varaprasad K et al (2011) Fabrication of curcumin encapsulated chitosan-PVA silver nanocomposite films for improved antimicrobial activity. *J Biomater Nanobiotechnol* 2:55–64. <https://doi.org/10.4236/jbnt.2011.21008>
- Wang X, Liu J, Wang P et al (2018) Synthesis of biomaterials utilizing microfluidic technology. *Genes (Basel)* 9:E283. <https://doi.org/10.3390/genes9060283>
- Wei W, Mao X, Ortiz LA, Sadoway DR (2011) Oriented silver oxide nanostructures synthesized through a template-free electrochemical route. *J Mater Chem* 21:432–438. <https://doi.org/10.1039/c0jm02214d>
- Yang CH, Wang LS, Chen SY et al (2016) Microfluidic assisted synthesis of silver nanoparticle–chitosan composite microparticles for antibacterial applications. *Int J Pharm* 510:493–500. <https://doi.org/10.1016/j.ijpharm.2016.01.010>
- Yousefzadeh S, Rajabi H, Ghajari N et al (2019) Numerical investigation of mixed convection heat transfer behavior of nanofluid in a cavity with different heat transfer areas. *J Therm Anal Calorim*. <https://doi.org/10.1007/s10973-019-09018-6>
- Zhou N, Li D, Yang D (2014) Morphology and composition controlled synthesis of flower-like silver nanostructures. *Nanoscale Res Lett* 9:1–6. <https://doi.org/10.1186/1556-276X-9-302>
- Zugic A, Tadic V, Savic S (2020) Nano- and microcarriers as drug delivery systems for usnic acid: review of literature. *Pharmaceutics*. <https://doi.org/10.3390/pharmaceutics12020156>

Publisher's Note Springer Nature remains neutral with regard to jurisdictional claims in published maps and institutional affiliations.